BBA - Molecular Cell Research 1871 (2024) 119721

Contents lists available at ScienceDirect

BBA - Molecular Cell Research

journal homepage: www.elsevier.com/locate/bbamcr

Research paper

E2F transcription factor-1 modulates expression of glutamine metabolic genes in mouse embryonic fibroblasts and uterine sarcoma cells

Katharina Huber [a,b], Albert Giralt [a], René Dreos [a], Helene Michenthaler [c], Sarah Geller [a], Valentin Barquissau [a], Dorian V. Ziegler [a], Daniele Tavernari [d,e,f], Hector Gallart-Ayala [g], Katarina Krajina [b], Katharina Jonas [b], Giovanni Ciriello [d,e,f], Julijana Ivanisevic [g], Andreas Prokesch [c,h], Martin Pichler [b,i], Lluis Fajas [a,*]

[a] Center for Integrative Genomics, University of Lausanne, Lausanne, Switzerland
[b] Division of Oncology, Department of Internal Medicine, Medical University of Graz, Graz, Austria
[c] Gottfried Schatz Research Center for Cell Signaling, Metabolism and Aging, Division of Cell Biology, Histology and Embryology, Medical University of Graz, Graz, Austria
[d] Department of Computational Biology, University of Lausanne, Lausanne, Switzerland
[e] Swiss Cancer Center Léman, Lausanne, Switzerland
[f] Swiss Institute of Bioinformatics, Lausanne, Switzerland
[g] Metabolomics Unit, Faculty of Biology and Medicine, University of Lausanne, Lausanne, Switzerland
[h] BioTechMed-Graz, Graz, Austria
[i] Translational Oncology, II. Med. Clinics, University Hospital of Augsburg, Augsburg, Germany

ARTICLE INFO

Keywords:
E2F1
SLC1A5
cancer metabolism
Glutamine
MYC
Uterine sarcoma

ABSTRACT

Metabolic reprogramming is considered as a hallmark of cancer and is clinically exploited as a novel target for therapy. The E2F transcription factor-1 (E2F1) regulates various cellular processes, including proliferative and metabolic pathways, and acts, depending on the cellular and molecular context, as an oncogene or tumor suppressor. The latter is evident by the observation that *E2f1*-knockout mice develop spontaneous tumors, including uterine sarcomas. This dual role warrants a detailed investigation of how E2F1 loss impacts metabolic pathways related to cancer progression.

Our data indicate that E2F1 binds to the promoter of several glutamine metabolism-related genes. Interestingly, the expression of genes in the glutamine metabolic pathway were increased in mouse embryonic fibroblasts (MEFs) lacking E2F1. In addition, we confirm that *E2f1*$^{-/-}$ MEFs are more efficient in metabolizing glutamine and producing glutamine-derived precursors for proliferation. Mechanistically, we observe a co-occupancy of E2F1 and MYC on glutamine metabolic promoters, increased MYC binding after E2F1 depletion and that silencing of MYC decreased the expression of glutamine-related genes in *E2f1*$^{-/-}$ MEFs. Analyses of transcriptomic profiles in 29 different human cancers identified uterine sarcoma that showed a negative correlation between E2F1 and glutamine metabolic genes. CRISPR/Cas9 knockout of E2F1 in the uterine sarcoma cell line SK-UT-1 confirmed elevated glutamine metabolic gene expression, increased proliferation and increased MYC binding to glutamine-related promoters upon E2F1 loss. Together, our data suggest a crucial role of E2F1 in energy metabolism and metabolic adaptation in uterine sarcoma cells.

1. Introduction

Cancer cells reprogram cellular metabolism to satisfy the demands of unrestrained growth and proliferation. Thus, metabolic reprogramming is considered as a hallmark of cancer and is clinically exploited for development of effective cancer therapeutics. This process enables cancer cells to adapt to intrinsic or extrinsic signals from the microenvironment by increasing the plasticity and flexibility in nutrient uptake and utilization. Rewiring of cancer metabolism involves several pathways such as increased aerobic glycolysis, imbalanced lipid synthesis, a shift toward pentose phosphate pathway, or elevated glutaminolysis [1,2].

* Corresponding author.
E-mail address: lluis.fajas@unil.ch (L. Fajas).

https://doi.org/10.1016/j.bbamcr.2024.119721
Received 27 October 2023; Received in revised form 12 March 2024; Accepted 27 March 2024
Available online 3 April 2024

Accumulating evidence supports the notion that glutamine metabolism is crucial in oncogenesis. Glutamine plays a versatile role in major biosynthetic pathways including tricarboxylic acid (TCA) cycle anaplerosis, nitrogen donation for nucleotide and hexosamine biosynthesis, precursor provision for glutathione production, lipid synthesis, glycolytic intermediates and amino acid synthesis [3].

Glutamine can be transported into the cell by membrane transporters such as neutral amino acid transporter member 5 (SLC1A5; also known as alanine-serine-cysteine transporter 2, ASCT2) [4]. Subsequently, glutamine can be catabolized to glutamate by intracellular glutaminases (GLS or GLS2) [5] and further to ketoglutarate (αKG) through glutamate dehydrogenase (GLUD1 or GLUD2) or aminotransferases glutamic-oxaloacetic transaminase (GOT1 or GOT2) or glutamate pyruvate transaminase (GPT1 or GPT2) and phosphoserine aminotransferase 1 (PSAT1), respectively [6]. αKG can enter the TCA for energy production and oxaloacetate (OAA) exiting the TCA cycle can be converted to aspartate to support nucleotide synthesis [7].

Cancer cells consume glutamine at a rate exceeding that of endogenous glutamine biosynthesis. Therefore, glutamine is currently considered essential in some cancer types [8] and identifying the molecular mechanisms implicated in the metabolic adaptation of cancer cells appears as a promising strategy for cancer therapy to overcome drug resistance [9].

Undoubtedly, cell cycle regulators are critical factors for cancer progression. Major components of the cell cycle machinery consist of cyclins, cyclin-dependent kinases (CDKs), CDK inhibitors of the CIP/KIP and INK_4 families, as well as the pocket proteins of the retinoblastoma family (pRB, p107, p130) and the E2 factor (E2F) family of transcription factors that comprise ten different members encoded by eight distinct genes (E2F1-E2F8) [10]. Upon mitogen activation, CDK4/6 and CDK2, with D-type and E-type cyclins respectively, sequentially phosphorylate the retinoblastoma proteins, thereby releasing E2F transcription factors [11]. The E2F transcription factors are the effectors of this pathway and regulate the expression of genes involved in various cellular processes such as cell cycle progression and cellular metabolism [12].

Alterations in one or more key components of the CDK-pRB-E2F axis occur frequently in most cancers (e.g. inactivation of pRB, overexpression of CDKs or inactivation of CDK inhibitors). Accordingly, an increase in E2F activity is commonly found in many human cancers [10]. However, depending on the cellular context and environmental conditions, E2F1 can function as an oncogene or a tumor suppressor gene as evidenced by the observation that *E2f1*-knockout mice develop spontaneous tumors [13,14]. In addition, copy number variation (CNV) analyses in human cancer types identified that loss of function mutations occur but at a low frequency (<10 % of cases affected) (https://portal.gdc.cancer.gov/genes/ENSG00000101412).

The CDK-pRB-E2F1 pathway has also been implicated in the regulation of the glutamine metabolism. Indeed, a link between pRB/E2F1 and redox metabolism, specifically an increase in the synthesis of the antioxidant glutathione from glutamine after pRB loss was demonstrated in advanced diseases [15]. In addition, in the context of pRB loss, glutamine metabolism is enhanced, partially through the direct control of glutamine uptake via specific E2F3-mediated transcription of target genes [16]. Moreover, Qui et al. demonstrated the contribution of F-Box Protein 4 loss and hyperactivation of cyclin D1-CDK4/6 kinases, which causes the phosphorylation-dependent inactivation of pRB, to glutamine addiction in human esophageal squamous cell carcinoma [17]. In sharp contrast, some studies showed that suppression of pRB phosphorylation by CDK4/6 inhibition is selectively associated with an increase in mitochondrial mass and mitochondrial metabolism fueled by an elevated glutamine metabolic flux in pancreatic cancer cells [18]. In line with this, CDK4/6 knockdown in HCT116 colorectal carcinoma cells increases mitochondrial metabolism through elevated utilization of glutamine and enhanced mitochondrial respiratory capacity [19]. Another study also showed that CDK4/6 inhibition by Palbociclib in A549 cells enhances glutaminolysis to maintain mitochondrial respiration and sensitizes A549 cell to the glutaminase inhibitor CB-839 [20]. In summary, whereas several studies reported that CDK4 inhibition led to metabolic rewiring including increased glutamine addiction [18–20], others clearly demonstrated that RB loss or increased CDK4 activity increased glutamine metabolism [16,17,21]. This discrepancy warrants a detailed molecular investigation of the molecular mechanism by which the CDK4/6-pRB-E2F pathway controls glutamine metabolism.

2. Methods

2.1. Cellular models and cell cultivation

Primary mouse embryonic fibroblasts (MEFs) were previously derived from *E2f1*$^{+/+}$ and

E2f1$^{-/-}$ mice (B6;129S4- E2f1$^{tm1\ Meg}$/J) [22,23] and immortalized by infection with the lentiviral vector SV40LargeTantigen.lti-neo encoding the SV40 large T antigen as described by Annibaldi et al. [24] MEFs were maintained in standard growth media (DMEM 41966-062, Thermo Fisher Scientific) supplemented with 10 % heat-inactivated fetal bovine serum (FBS, SV30160.03, Lot No. RB35956, HyClone, GE Healthcare Life Sciences) at 37 °C in a 5 % CO_2 incubator. For RNA-seq experiments, MEFs were cultivated with DMEM without glucose, glutamine, phenol red, and sodium pyruvate (A14430-01, Thermo Fisher Scientific) supplemented with 10 % dialyzed and filtered FBS (26-400-044, Thermo Fisher Scientific), and either 25 mM glucose (G8769, Sigma-Aldrich) and 4 mM glutamine (25030-024, Thermo Fisher Scientific), and either 25 mM glucose (G8769, Sigma-Aldrich) and 4 mM glutamine (25030-024, Thermo Fisher Scientific) or only 4 mM glutamine for 16 h.

SK-UT-1 (uterus, leiomyosarcoma) cells were derived from ATCC (HTB-114) and cultured in DMEM/F12 media (21331020, Thermo Fisher Scientific) supplemented with 10 % heat-inactivated fetal bovine serum (FBS, SV30160.03, HyClone, GE Healthcare Life Sciences), 2 mM glutamine (25030-024, Thermo Fisher Scientific) and Penicillin-Streptomycin (15140163, Thermo Fisher Scientific) at 37 °C in a 5 % CO_2 incubator.

Cells were routinely monitored and confirmed to be free of mycoplasma.

2.2. RNA isolation, reverse transcription, and gene expression analysis

To investigate gene expression, primary MEFs or SV40 immortalized MEFs were plated in triplicates in 60 mm dishes (430,166, Corning) in 4 mL standard growth media. After 24 h, MEFs were washed once with 4 mL D-PBS (14,190,169, Thermo Fisher Scientific) and RNA was isolated using the TRI reagent (T9424, Sigma-Aldrich, Thermo Fisher Scientific) according to the manufacturer's protocols. RNA concentrations were determined with a NanoDrop 8000 (Thermo Fisher Scientific). Reverse transcription for cDNA generation was performed using the SuperScript™ II Reverse Transcriptase (8064-014, Invitrogen, Thermo Fisher Scientific). mRNA expression was assessed using real-time PCR on the QuantStudio™ 6 real-time PCR system (Applied Biosystems, Thermo Fisher Scientific) and SYBR Green detection (04913914001, Roche). Gene expression was normalized to GeoMean of housekeeping genes *Tbp, Rs9* and *Actb*. Relative mRNA expression levels were calculated using the 2^(Delta Ct) method [25]. For primer sequence see Supplementary table 2.

2.3. Cell lysis for protein extraction, determination of protein concentration and Western blot

To extract proteins from SV40 immortalized *E2f1*$^{+/+}$ and *E2f1*$^{-/-}$ MEFs, cells were cultured in 60 mm dishes, washed twice with 4 mL D-PBS and scraped down in M-PER protein lysis buffer (78,501, Thermo Fisher Scientific) supplemented with 1× Halt™ Phosphatase (78,426,

Thermo Fisher Scientific) and 1× Halt™ Protease inhibitor cocktail (78,429, Thermo Fisher Scientific). Afterwards, cell lysates were incubated for 30 min on ice, followed by 3 times 5 cycles of sonication (30 s ON, 30 s OFF) using the Bioruptor® Plus (Diagenode). After centrifugation (10,000 rpm, at 4 °C for 5 min), protein lysate was transferred into a new 1.7 mL tube and stored at −20 °C until further usage. Protein concentration was determined using the Pierce BCA Protein Assay Kit (23,225, Thermo Fisher) according to the manufacturer's protocol. Thereafter, 10–20 μg of protein were subjected to 10 % SDS-gel, which were blotted to nitrocellulose membranes (1,620,115, Bio-Rad). Reversible staining of protein bands was confirmed using Ponceau S (P3504, Sigma-Aldrich, Merck) or reversible protein stain kit (24,580, Thermo Fisher Scientific). The following antibodies were used in 5 % skim milk (232,100, BD) dissolved in Tris-buffered saline containing 0.05 % Tween 20 (A1389,0500, AppliChem): E2F1 (3742, Cell Signaling Technology) and Anti-α- TUBULIN (T6199, Sigma Aldrich, Merck). After incubation with corresponding HRP-linked secondary anti-mouse IgG (7076P2, Cell Signaling Technology) or anti-rabbit IgG HRP-linked antibody (7074P2, Cell Signaling Technology), luminescence intensity was captured by a Fusion FX imager (Vilber) and quantified by densitometry using Fiji (version 2.3.0). Expression levels of proteins of interest were normalized to TUBULIN protein amount.

Total proteins from SK-UT-1 cells were isolated and separated as described previously [26]. The following primary antibodies were used: E2F1 (#3, Cell Signaling Technology, Cambridge, United Kingdom) diluted 1:1000, and the housekeeper Cofilin (ab42824, Abcam, Cambridge, United Kingdom) diluted 1:10,000.

2.4. RNA-seq

RNA was extracted as described above from 4 SV40 immortalized *E2f1*$^{+/+}$ and *E2f1*$^{-/-}$ MEFs from 4 independent experiments. RNA quality was assessed on a Fragment Analyzer (Agilent Technologies) and all RNAs had a RQN above 9.3. RNA-seq libraries were prepared from 500 ng of total RNA with the Illumina TruSeq Stranded mRNA reagents (Illumina) using a unique dual indexing strategy, and following the official protocol. Libraries were quantified by a fluorimetric method (QubIT, Life Technologies) and their quality assessed on a Fragment Analyzer (Agilent Technologies). Sequencing was performed on an Illumina NovaSeq 6000 for 100 cycles single read. Sequencing data were demultiplexed using the bcl2fastq2 Conversion Software (version 2.20, Illumina).

2.4.1. RNA—seq data analysis

Reads were mapped on the mouse genome GRCm38 (Ensembl version 91) using STAR v.2.7.0f [27] with the following settings: options: –outFilterType: BySJout, –outFilterMultimapNmax 20 –outMultimapperOrder Random –alignSJoverhangMin 8 –alignSJDBoverhangMin 1 –outFilterMismatchNmax 999 –alignIntronMin 20 –alignIntronMax 1000000 –alignMatesGapMax 1000000). Read counts in genes loci were evaluated with htseq-count [28] (v. 0.13.5). Differential expression analysis was done in R (v4.1.1) using DESqe2 package [29] with adjusted p-valued for multiple testing (Benjamini-Hochberg procedure). PCA was performed in R using variance stabilized expression data for the top 500 more variable genes. Gene set enrichment analysis was done in R using MsigDB [30] and *fgsa* Bioconductor package [31]. KEGG and GO enrichment analysis was done in R using *ReactomePA* Bioconductor package [32].

2.5. Metabolomics

2.5.1. Sample preparation

SV40 immortalized MEFs were plated in 15 cm dishes (430,599, Corning, 6 replicates per condition) in standard growth media (41965-062, Thermo Fisher Scientific) supplemented with 10 % heat inactivated FBS (HyClone, GE Healthcare Life Sciences, #SV30160.03, Lot.No: RB35956). After plating, cells were allowed to equilibrate for 24 h before 4 h treatment with 4 mM L-glutamine $^{13}C_5$ (605,166, Merck). Cells were extracted by the addition of cold MeOH:H2O (4:1). The extracts were centrifuged at 14,000 rpm at 4 °C for 15 min and the resulting supernatant was transferred to LC-MS vials for injection [33].

2.5.2. Data acquisition – LC-HRMS analysis

Cell extracts were analyzed by Hydrophilic Interaction Liquid Chromatography coupled to high resolution mass spectrometry (HILIC - HRMS) in negative ionization mode using a 6550 Quadrupole Time-of-Flight (Q-TOF) system interfaced with 1290 UHPLC system (Agilent Technologies) as previously described [34]. A SeQuant ZIC-pHILIC (100 mm, 2.1 mm I.D. and 5 μm particle size, Merck) column was used for metabolite separation. The mobile phase was composed of A = 20 mM ammonium Acetate and 20 mM NH4OH in water at pH 9.7 and B = 100 % ACN. The linear gradient elution was from 90 % (0–1.5 min) to 50 % B (8–1L min) down to 45 % B (12–15 min). Finally, the initial chromatographic conditions were established during a 9 min post-run for column re-equilibration. The flow rate was 300 μL/min, column temperature 30 °C and sample injection volume 2 μL. Mass spectrometry ESI source conditions were set as follows: dry gas temperature 290 °C and flow 14 L min^{-1}, fragmentor voltage 380 V, sheath gas temperature 350 °C and flow 12 L min^{-1}, nozzle voltage 0 V, and capillary voltage −2000 V. The instrument was set to acquire over the full *m/z* range 50–1000 with the MS acquisition rate of 2 spectra/s. In addition, AIF (all ion fragmentation) MS/MS analysis were performed on pooled QC samples at a collision energy (CE) of 0, 10 and 30 eV.

2.5.3. Data (pre)processing

Raw LC/MS files was processed using Profinder B.08.00 software (Agilent Technologies) and the targeted data mining in isotopologue extraction mode for metabolite annotation based on an *in-house* database containing around 600 polar metabolites (analyzed in the same analytical conditions). Metabolites will be identified based on accurate mass and retention time using the parameters settings as follows: mass accuracy tolerance 10 ppm, retention time tolerance 0.2 min, height filter 1000 counts, peak spectrum obtained as an average of scans at 10 % of the peak maximal height. The relative quantification of metabolites was based on EIC (Extracted Ion Chromatogram) areas. The correction for natural isotope abundance was integrated in ProFinder [35]. The obtained tables, containing peak areas of detected metabolites across all samples, were exported to "R" software http://cran.r-project.org/ and signal intensity drift correction was done within the LOWESS/Spline normalization program [35] followed by noise filtering (CV (QC features) > 30 %). Finally, the metabolite abundance was reported to total protein content (measured in the cell pellet using BCA assay, Thermo Fisher Scientific).

2.5.4. Metabolite identification

Short listed ions of interest were matched against the *in-house* created Accurate Mass Retention Time (AMRT) database. The identity of these putatively identified metabolites was further confirmed using the fragmentation (MS/MS data) pattern matching against METLIN standard spectral library [36].

2.5.5. Exploratory statistical analysis of label incorporation

The label incorporation or ^{13}C ##enrichment was calculated based on relative isotopolgue abundances in two different conditions [37,38]. The univariate analysis (on $\log_{10}$ transformed data) was applied to test the significance of label enrichment and changes in metabolite levels in different conditions (p-value = 0.05 followed by the Benjamini-Hochberg correction for multiple testing).

2.5.6. Data visualization

GraphPad prism software (v9.4.1) has been used to create bar charts.

2.6. Cell proliferation: Cy-quant assay

SV40 immortalized E2f1$^{+/+}$ and E2f1$^{-/-}$ MEFs were plated in replicates ($n = 6$ / dish) in 96-well dishes (3599, Corning), with an initial seeding density of 2000 cells per well in DMEM (41966–062, Thermo Fisher Scientific) supplemented with 10 % heat-inactivated FBS (SV30160.03, Lot No. RB35956, HyClone, GE Healthcare Life Sciences). After seeding, cells were allowed to equilibrate overnight (16 h) and one 96-well dish was washed once with PBS and immediately frozen at −80 °C to quantify the starting cell number prior to treatment. The wells in the remaining dishes were washed twice with PBS and media was replaced by DMEM no glucose, no glutamine, no phenol red (A14430–01, Thermo Fisher Scientific) supplemented with 10 % dialyzed and filtered FBS (26400–044, Thermo Fisher Scientific), and either 25 mM glucose (G8769, Sigma-Aldrich) and 4 mM glutamine (25030–024, Thermo Fisher Scientific) or only 4 mM glutamine. The media was changed every 24 h. Final cell counts were determined 1–4 days after the initial treatment using the CyQuant assay (C7026, Thermo Fisher Scientific) according to manufacturer's instructions.

2.7. ChIP- Seq tracs

The genome-wide occupancy of E2F1 in the genomic sequences of genes involved in glutamine metabolism in human cervical cancer cell line (HeLa) and human breast cancer cell line (MCF7) were analyzed using custom tracks from published ChIP-Seq datasets available from the UCSC genome browser (http://genome.ucsc.edu). Data were illustrated using the integrative genomics viewer (version 2.5.3, https://software.broadinstitute.org/software/igv/).

2.8. ChIP-qPCR

Chromatin was prepared from SV40 immortalized E2f1$^{+/+}$ and E2f1$^{-/-}$ MEFs crosslinked with 1 % formaldehyde in PBS for 10 min at room temperature and the reaction was stopped by adding glycine to a final concentration of 0.125 M for 2 min at room temperature. Crosslinked cells were rinsed twice with PBS, collected with a cell scraper, resuspended in cell lysis buffer (10 mM Tris-HCl pH 8.1, 10 mM NaCl, 1.5 mM $MgCl_2$, 0.5 % NP-40), supplemented with 1× Halt™ Protease inhibitor cocktail (78,429, Thermo Fisher Scientific) and collected in 1.5 mL DNA-low binding tubes to remove the cytoplasmic fraction. Nuclei were resuspended in nuclei lysis buffer (50 mM Tris-Cl pH 8.0, 1.5 mM EDTA, 1 % SDS), and lysate was sonicated for 30 cycles (30 s ON/30 s OFF) in a Diagenode Bioruptor (UCD-300, Diagenode). The sonicated and diluted chromatin was pre-cleared with protein A agarose / salmon sperm DNA (16–157, EMD Millipore) for 30 min at 4 °C with agitation according to the manufacturer's protocol and afterwards incubated with 4 μg immunoprecipitating antibody (c-MYC ab32072, Abcam) and in parallel one chromatin sample with the negative control (normal rabbit IgG, 2729, Cell Signaling Technology). IP samples were rotated overnight at 4 °C and pull-down was performed with 60 μL protein A agarose / salmon sperm DNA for 1 h at 4 °C with agitation according to the manufacturer's protocol. The protein A agarose/antibody/DNA complex was washed for 5 min on a rotating platform with 1 mL of each of the buffers (low salt wash buffer: 50 mM Tris pH 7.5, 150 mM NaCl, 1 % Triton 100×, 0.1 % SDS, 1× protease inhibitor, 1 mM EDTA; high salt wash buffer: 50 mM Tris pH 7.5, 500 mM NaCl, 1 % Triton 100×, 0.1 % SDS, 1× protease inhibitor, 1 mM EDTA; LiCl wash buffer: 20 mM Tris pH 7.5, 250 mM LiCl, 1 % NP40, 1 % deoxycholic acid, 1× protease inhibitor, 1 mM EDTA; TE buffer: 10 mM Tris pH 7.5, 1 mM EDTA) and centrifuge (1000 rpm, 4 °C, 2 min). To elute the DNA complex from the antibody, two times 50 μL of elution buffer (0.1 M $NaHCO_3$, 1 % SDS) were added and incubated each time at 37 °C for 15 min. Combined eluates as well as 10 % input samples were reversed crosslinked by adding 0.25 M NaCl, 2 μL RNase A (10 mg/ml, R6513, Sigma-Aldrich) and incubated at 65 °C overnight, followed by incubation with 2 μL of proteinase K (20 mg/ml, Roche) for 1 h. DNA was purified using the Qiagen MinElute reaction cleanup kit (28,026, Qiagen). ChIP-qPCR was performed using the SYBR Green Master Mix (04913914001, Roche) on the QuantStudio™ 6 real-time PCR system (Applied Biosystems, Thermo Fisher Scientific). For primer sequence see Supplementary table 2.

2.9. MYC-silencing in MEFs

siRNA-mediated gene knockdown in SV40 MEFs was achieved using 30 nM of a mix of 2 control siRNAs (SIC001 and SIC002, Sigma-Aldrich), or 30 nM of esi-RNA targeting *Myc* (EMU075291, Sigma-Aldrich). One day before transfection, 50,000 cells were plated in 6 cm dish and transfection was performed using Lipofectamine RNAiMax transfection reagent (13,778,075, Thermo Fisher Scientific) according to manufacturer's protocols. Cells were harvested 24 h post transfection. RNA was extracted as described above. MYC silencing was confirmed by qPCR.

2.10. E2F1-silencing in SK-UT-1

siRNA-mediated gene knockdown in 2×10^5 / 6-well SK-UT-1 was achieved using 20 nM of Allstar negative control siRNAs (1,027,281, Qiagen), or 20 nM of Flexitube si-RNA targeting human E2F1 (SI00073976, Qiagen). Fast-forward transfection was performed according to the manufacturer's instructions (HiPerFect transfection reagent 1,029,975, Qiagen). Cells were harvested 48 h post transfection according to TRIzol user guide (15,596,026, Thermo Fisher Scientific) and 1 μg of total RNA was reversely transcribed with the QuantiTect reverse transcription kit (205,310, Qiagen). RT-qPCR was performed on the LightCycler 480 (Roche) using the QuantiTect SYBR Green PCR Kit (204,145, QIAGEN).

2.11. E2F1 knockout in SK-UT-1 using CRISPR/Cas9 technology

E2F1 knockout SK-UT1 cell lines have been generated using CRISPR/Cas9 technology as previously descripted in the protocol of Kahn et al. [39] Targeting guides (targeting sequence: 5'-TCCCAAGGTCCTGACACGTCACGT-3') were designed using CRISPick (https://portals.broadinstitute.org/gppx/crispick/public).

2.12. WST-1 cell growth assay

To assess the impact of E2F1 on cellular growth, $2{,}5 \times 10^3$ LacZ pool, E2F1-ko clone 2 or E2F1-ko clone3 SK-UT1 cells were plated in a 96-well plate (8 replicates, one plate for each time point). Cells were cultivated for 24, 48, 72, and 96 h. At each time point, WST-1 proliferation reagent (Roche) was added to the wells in a 1:10 ratio according to the manufacturer's instructions. Plates were incubation at 37 °C for 120 min and colorimetric changes were measured using a SPECTROstar Omega (BMG Labtech, Ortenberg, Germany) at a wavelength of 450 nm with a reference wavelength of 620 nm.

2.13. Nuclei isolation and CUT&RUN-qPCR

CUT&RUN (Cleavage Under Targets and Release Using Nuclease) experiments were carried out following nuclei isolation in a glass douncer (9.651616, Bartelt) using ice-cold nuclei isolation buffer (10 mM Tri-HCl pH 7.5, 2 mM $MgCl_2$, 3 mM $CaCl_2$, 1 % Igepal, 10 % glycerol) and centrifugation at 600 xg for 5 min at 4 °C to pellet the nuclei. Nuclei were washed two times with wash buffer (20 mM HEPES, 150 mM NaCl, 0,5 mM spermidine trihydrochloride (S2501-5G, Sigma-Aldrich) supplemented with EDTA-free protease inhibitor cocktail (4693116001, Sigma-Aldrich) before counting. CUT&RUN was performed according to the published CUT&RUN protocol [40] starting with $0{,}75 \times 10^6$ nuclei. Nuclei were bound to activated concanavalin-A beads (21–1401-EPC, BioCat) while rotating for 10 min at RT and

incubated with 0,75 ng (c-MYC ab32072, Abcam) or isotype control (rabbit IgG, 2729, Cell Signaling Technology) for 3 h at 4 °C. To fragment the DNA, beads were washed and incubated for 1 h at 4 °C in wash buffer containing 1 µg/mL p-MNAse (15-1016-EPC, BioCat). After activation by Ca^{2+} at 4 °C for 30 min, 2× STOP buffer (340 mM NaCl, 20 mM EDTA, 4 mM EGTA, 50 µg/mL RNAseA (R6513, Sigma-Aldrich), 50 µg/mL glycogen (10,814,010, Thermo Scientific) was added to the reaction and incubated at 37 °C for 10 min to release the fragmented DNA from the insoluble nuclear chromatin. DNA extraction was carried out using phenol-chloroform-isoamyl alcohol 25:24:1 (PCI; 15593031, Invitrogen, Thermo Fisher Scientific) method according to manual. The pellet was washed with 100 % ethanol and dissolved in 50 µL ddH2O [41]. DNA concentrations were determined with a Qubit 4 Fluorometer (Life Technologies) before DNA fragments were amplified using Blue SybrGreen qPCR Mastermix (331416XL, Biozym Scientific). CUT&RUN data show means of $2^{(Delta\ Ct)}$ method, normalized to HPRT1 and VCAM1 control loci, as well as to the corresponding IgG control. For primer sequences see Supplementary table 2.

2.14. Co-regulatory network and motif analyses

E2F1 co-regulatory network analysis was perform using ChIP-seq ENCODE data for HeLa-S3 cell line (67 transcription factors) downloaded from the ENCODE website (https://genome.ucsc.edu/) and analyzed as followed: Gene promoters (from EPDnew [42], 2 kb region upstream the TSS) with E2F1 binding sites were studied for the presence of other transcription factor (TF) binding sites (co-occurrence). First, the co-occurrence frequency of each TF with E2F1 was calculated (number of promoters with both E2F1 binding sites and target TF; versus the total number of promoters with E2F1 binding sites). Then, the co-occurrence frequency was compared to the inverse frequency (calculated with a bootstrap subsampling approach: frequency of E2F1 binding sites on a random selection of promoters with target TF binding sites, repeated 100 times). The difference between co-occurrence and inverse frequencies was then calculated and normalized by the inversed frequency. This analysis was restricted to Cell Cycle genes (KEGG id: hsa04110) and Alanine Aspartate Glutamate Metabolism genes (KEGG id: hsa00250). Finally, the presence of E2F family and MYC binding sites in genes promoters from these two pathways were clustered hierarchically (euclidean distance).

2.15. Computational analyses of the cancer genome atlas patient datasets

Datasets containing normalized bulk transcriptomic profiles of 29 tumor types generated with RNA-seq by The Cancer Genome Atlas (TCGA) consortium were downloaded from GDC data portal (https://portal.gdc.cancer.gov/) and cBioPortal (https://www.cbioportal.org/) [43], along with clinical information. The gene set constituting the glutamine signature was retrieved from the KEGG database (entry: 'hsa00250', name: 'Alanine, aspartate and glutamate metabolism - *Homo sapiens* (human)') [44]. In a second analysis, the KEGG hsa00250 gene list was restricted to genes, which are direct E2F1 and MYC targets and were differentially expressed as indicated by the RNA-seq experiment (Supplementary table 1). The signature scores of each tumor transcriptome were computed with R package 'singscore' v1.12.0 [45]. Survival analyses were performed with the R package 'survival' v3.2–13 [46], with *p*-values computed using log-rank test. All computational analyses were implemented in R version 4.1.1.

2.16. Statistical analysis

Results are illustrated as mean ± standard deviation (SD) or standard error of the mean (SEM) of at least three replicates if not indicated otherwise. Statistical significance was determined using the unpaired two-tailed student's *t*-test. Statistical analyses were carried out using the Prism software (GraphPad, v9.5.1). Normal distribution was assessed by Shapiro-Wilk normality test and further analyzed using a Student t-test (normal distribution) or a Mann-Whitney *U* test or an ordinary one-way ANOVA with Holm-šidák's multiple comparison (normal distribution) or Kurskal-Wallis test with Dunnett's multiple comparisons test and defined as $*p \leq 0.05$; $**p \leq 0.01$; $***p \leq 0.001$; $****p \leq 0.0001$).

3. Results

3.1. E2F1 regulates the expression of the glutamine transporter Slc1a5 and genes in the glutamine metabolic pathway

Previously, it was found that loss of E2F1 in mice results in tumorigenesis, demonstrating that E2F1 can also function as a tumor suppressor [13,14]. If E2F1's function in metabolic rewiring contributes to tumor formation in mice has not been investigated in detail.

Immortalized embryonic fibroblasts (MEFs) were isolated from *E2f1*-wild-type (*E2f1*$^{+/+}$) and *E2f1*- knock-out (*E2f1*$^{-/-}$) mice (Fig. 1 A-C) and used as a genetic tool to determine the gene expression profiles of metabolic pathways underlying E2F1 regulation by RNA-seq analysis. 2143 genes were identified differentially expressed in *E2f1*$^{-/-}$ versus *E2f1*$^{+/+}$ MEFs (561 upregulated, 1582 downregulated) by gene expression profiling. Among them was the glutamine transporter *Slc1a5,* which was one of the most significantly upregulated genes in *E2f1*$^{-/-}$ MEFs (Fig. 1D). KEGG pathway analysis indicated changes in several metabolic pathways including oxidative phosphorylation, which has been previously related to E2F1 activity [47]. Interestingly, alterations in specific metabolic pathways comprising amino acid metabolism were detected (Supplementary Fig. 1A). A subset of these altered genes belongs to the glutamine family of amino acid metabolism-related genes, which were significantly upregulated in *E2f1* knockout MEFs identified by RNA-Seq (Fig. 1E). Together, these data reveal the transcriptional networks that are disturbed by E2F1 depletion and highlight the upregulation of metabolic pathways that are known to be involved in tumor development and progression, such as glutamine metabolism.

(A) Analysis of *E2f1* mRNA expression (B) and E2F1 protein expression in SV40-immortalized mouse embryonic fibroblasts (MEFs). (C) Quantification of western blot signal from B using ImageJ. $n = 3$. All data shows mean ± SD. (D) Volcano plot representing alterations in gene expression upon *E2f1* knockout in SV40 immortalized MEFs. (E) Gene expression in *E2f1*$^{+/+}$ and *E2f1*$^{-/-}$ SV40-immortalized MEFs from RNA-seq data shown as z-score. * padj ≤0.05, ** padj ≤0.01, *** padj ≤0.001, **** padj ≤0.0001 were derived from differential expression analysis carried out in R using DESeq2 and FDR corrected using Benjamini Hochberg correction.

3.2. Reprogramming of metabolism upon E2f1 deletion

Next, the metabolic consequences of the increased expression of genes that participate in the glutamine metabolic pathway in MEFs were determined. Steady-state metabolomic analysis was performed in *E2f1*$^{+/+}$ and *E2f1*$^{-/-}$ MEFs and identified significantly upregulated metabolites related to glutamine metabolism in the absence of E2F1. Moreover, glutamine levels were significantly decreased in *E2f1*$^{-/-}$ MEFs. These data indicated a role of E2F1 in regulating several amino acid metabolic pathways and suggested an increase in the glutamine catabolism, which is required for the biosynthesis of amino acids such as creatine, proline, aspartate, and glutathione in *E2f1*$^{-/-}$ MEFs (Fig. 2A). Moreover, the analysis of the glutamine metabolic flux using [U—$^{13}C_5$]-glutamine as a tracer (Fig. 2B - C), showed a direct contribution of glutamine to the biosynthesis of glutamate m5, α-ketoglutarate (αKG) m5, succinate m4, fumarate m4, and malate m4, demonstrating both enhanced glutamine oxidation and the consequent carbon contribution to the oxidative TCA cycle (Fig. 2D). Interestingly, *E2f1*$^{-/-}$ MEFs presented elevated levels of aspartate m3, and malate m3 (Fig. 2E), revealing a more active reductive carboxylation. Nevertheless, the relative proportion of aspartate m3 and malate m3 versus aspartate m4, and malate m4-labeled species

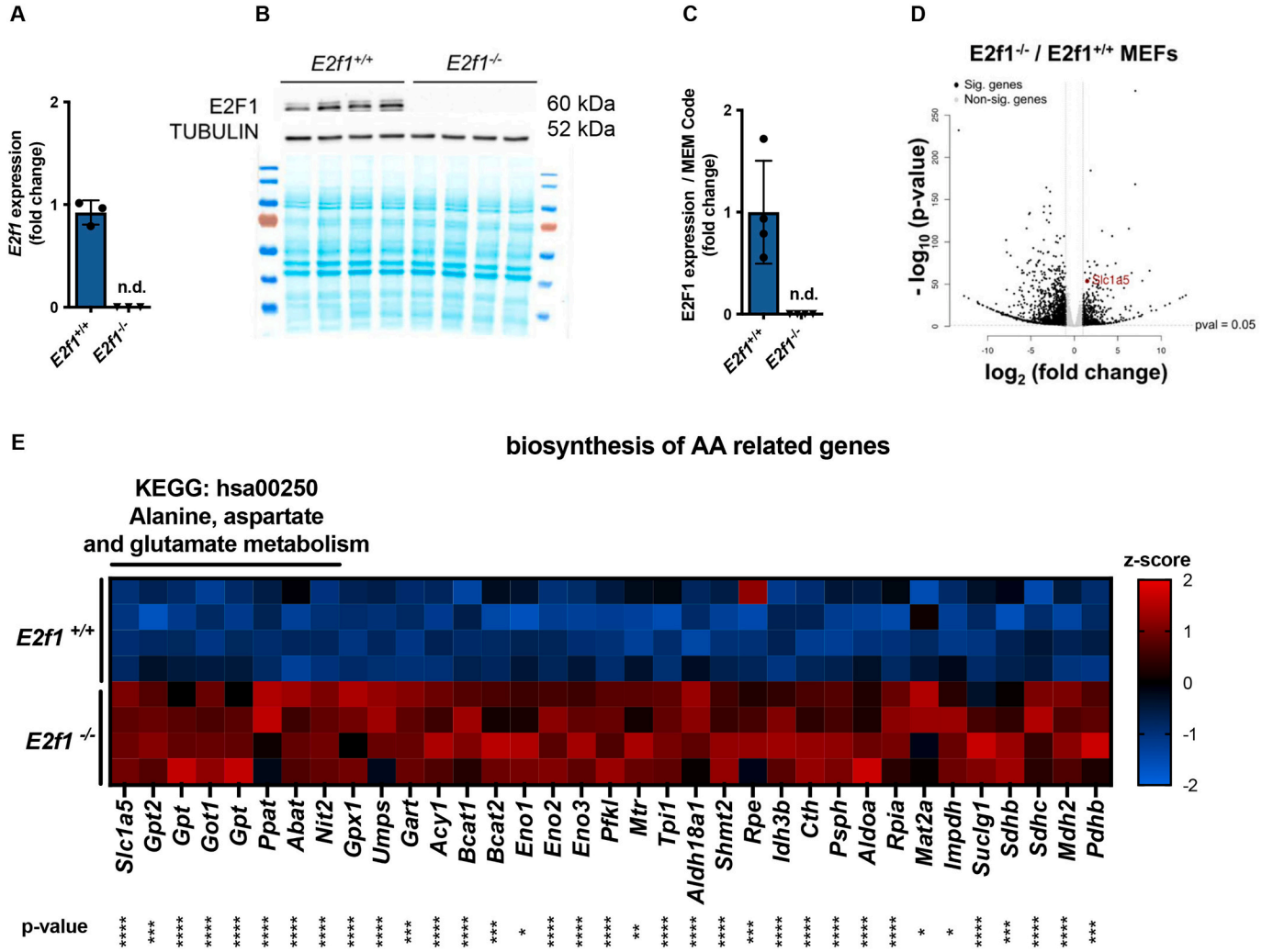

Fig. 1. E2F1 regulates the expression of glutamine metabolic target genes.

indicated that oxidative TCA cycle was the main pathway of the glutamine metabolism, shown by the similar labeling pattern of total carbon contribution (Fig. 2F). In contrast, *E2f1*$^{+/+}$ MEFs demonstrated an increase in label enrichment of αKG m3, succinate m2 and malate m2, suggesting higher incorporation of glucose-derived pyruvate into the TCA intermediates (Supplementary Fig. 2D). Besides the elevated glutamine turnover and incorporation into oxidative TCA cycle in *E2f1*$^{-/-}$ MEFs, we also found a higher contribution of glutamine to glutathione, proline, and asparagine levels (Fig. 2G) pointing to the enhanced incorporation of glutamine into additional glutamine consuming pathways. This increased glutamine metabolic fluxes were accompanied by increased ATP levels detected in *E2f1*$^{-/-}$ MEFs (Supplementary Fig. 2A-C). Together, these data identified metabolic control and reprogramming of glutamine metabolism upon E2F1 depletion and indicate that *E2f1*$^{-/-}$ MEFs are more efficient in metabolizing glutamine, thereby producing important intermediates for cellular proliferation.

(A) Quantification of intracellular metabolites related to glutamine metabolism. Data are normalized by cell number and represented as fold change (FC) relative to control cells for each metabolite. (B) Schematic of labeling strategy, using [U—$^{13}C_5$]-glutamine. SV40-immortalized MEFs were cultured for 4 h in the presence of tracer [U—$^{13}C_5$]-glutamine, followed by mass spectrometry of the indicated metabolites. (C) Schematic representation of the labeling distribution of [U-$^{13}C_5$]-glutamine into the TCA intermediates in the first turn of the TCA cycle considering oxidative TCA cycle (red labeling) and reductive carboxylation (green labeling). (D-E) Glutamine contribution to the TCA cycle intermediates in SV40-immortalized *E2f1*$^{+/+}$ and *E2f1*$^{-/-}$ MEFs. TCA intermediates were isolated from cells for isotopologue distribution analysis. (D) Normalized m5 glutamate (Glu), m4 citrate (Cit), m5 α-ketoglutarate (αKG), m4 succinate (Suc), m4 fumarate (Fum), m4 malate (Mal) and m4 aspartate (Asp) labeling obtained through oxidative TCA pathway of [U-$^{13}C_5$]-glutamine. Values are normalized to total label enrichment (∑m). (E) Normalized m5 citrate, m3 aspartate, and m3 malate are indicative for reductive carboxylation of [U-$^{13}C_5$]-glutamine. Values are normalized to total label enrichment (∑m). (F) Total percentage of carbons for each TCA metabolite. (G) Total percentage of carbon contribution for indicated amino acids. Shown values are mean ± SD of $n = 6$ technical replicates. Significance was determined by Holm-šidák's multiple comparison. Statistically significant differences between SV40-immortalized *E2f1*$^{+/+}$ and *E2f1*$^{-/-}$ MEFs are indicated as $p < 0.05$ (*), $p < 0.01$ (**), $p < 0.001$ (***) and $p < 0.0001$ (****).

3.3. Regulation of glutamine metabolism by E2F1 affects proliferation capacity

Previously, it was found that loss of E2F1 in mice results in tumorigenesis, demonstrating that E2F1 can also function as a tumor suppressor [13,14]. Our results of increased cellular proliferation are

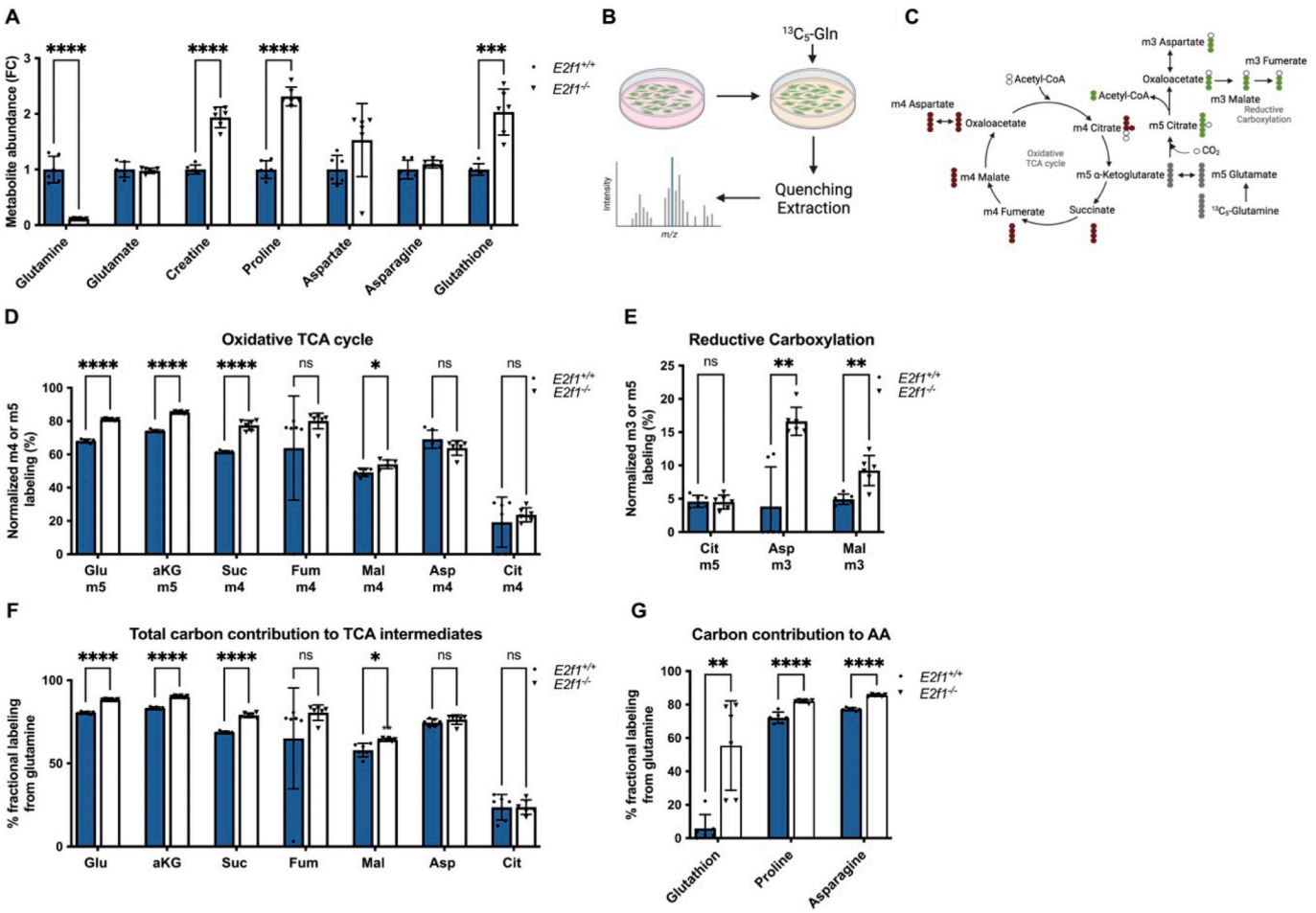

Fig. 2. Increased glutamine metabolism upon loss of E2F1 in MEFs.

consistent with the previous finding, showing that loss of *E2f1* increased the proliferation of the *E2f1*$^{-/-}$ compared to *E2f1*$^{+/+}$ SV40-immortalized MEFs [48] (Fig. 3A). Glucose and glutamine are two main sources for carbon fuel in proliferating cells [49]. To assess if the efficient metabolization of glutamine in *E2f1*$^{-/-}$ MEFs can provide them a growth advantage, cells were cultured in media withdrawn of glucose and in the presence of high glutamine concentration. Indeed, *E2f1*$^{-/-}$ MEFs continued to proliferate (albeit much more slowly compared to standard growth media), whereas *E2f1*$^{+/+}$ MEFs lost viability without glucose over a time course of 72 h (Fig. 3B-E). To investigate how *E2f1*$^{-/-}$ MEFs can adapt to glucose starvation conditions by increasing glutamine metabolism, we carried out gene expression profiles in cells derived from media without glucose for 16 h and identified that glutamine metabolic genes were significantly upregulated in *E2f1*$^{-/-}$ MEFs compared to *E2f1*$^{+/+}$ MEFs (Fig. 3F).

Together, these results confirm increased proliferation upon E2F1 loss, which partly dependents on glutamine metabolism.

(A-E) Proliferation rate of SV40-immortalized *E2f1*$^{+/+}$ and *E2f1*$^{-/-}$ MEFs was determined in the presence or absence of glucose. (A-B) Cell counts, normalized to cell number at $t = 0$ when treatment media were applied, were assessed over a time course of 72 h and (Fig. 3C-E) used to calculate proliferation rate. Data are shown as mean ± SD of $n = 8$ technical replicates illustrating one representative experiment out of three. Statistical significance was determined using ordinary one-way ANOVA with multiple comparisons and defined as $p < 0.05$ (*), $p < 0.01$ (**), and $p < 0.0001$ (****). (F) Gene expression in SV40-immortalized *E2f1*$^{+/+}$ and *E2f1*$^{-/-}$ MEFs from RNA-seq data shown as z-score (light green to dark green). * padj ≤0.05, ** padj ≤0.01, **** padj ≤0.0001 were derived from differential expression analysis carried out in R using DESeq2 and FDR corrected using Benjamini Hochberg correction.

3.4. *E2F1 binds to the promoter of the glutamine transporter Slc1a5 and of glutamine metabolic genes*

To investigate if E2F1 could directly regulate the expression of these metabolic pathways, gene ontology (GO) analysis on biological processes using published ChIP-Seq datasets (http://genome.ucsc.edu) was performed, which revealed that pathways related to glutamine metabolism were enriched in genes that contain an E2F1 binding site in the promoter region (data not shown) and confirmed a direct binding of E2F1 to the promoter of glutamine metabolic genes, including the glutamine transporter *SLC1A5* (Fig. 4A). In order to elucidate the molecular mechanisms underlying the observed increase in the expression of glutamine metabolic genes in *E2f1*$^{-/-}$ MEFs, the hypothesis was tested if in the absence of E2F1, other transcription factors (TF) regulate the expression of glutamine metabolic genes in the proximity of the *E2f1* binding site in the promoter of these genes. Therefore, to uncover E2F1 co-regulatory networks specifically on glutamine metabolic gene promoters compared to cell cycle gene promoters, ChIP-seq experiments including 61 unique TF in HeLa cells (ENCODE project) were used. Using these processed data, the co-occurrences of E2F1 with other TFs was uncovered. These analyses identified MYC as a factor that shows a high co-occurrence with E2F1 specifically on the promoter of glutamine metabolic genes compared to the promoters of cell cycle genes (Fig. 4B). To further investigate if these changes in glutamine metabolic gene expression were likely to be regulated by increased MYC binding after E2F1 depletion, MYC binding to the promoter of the glutamine

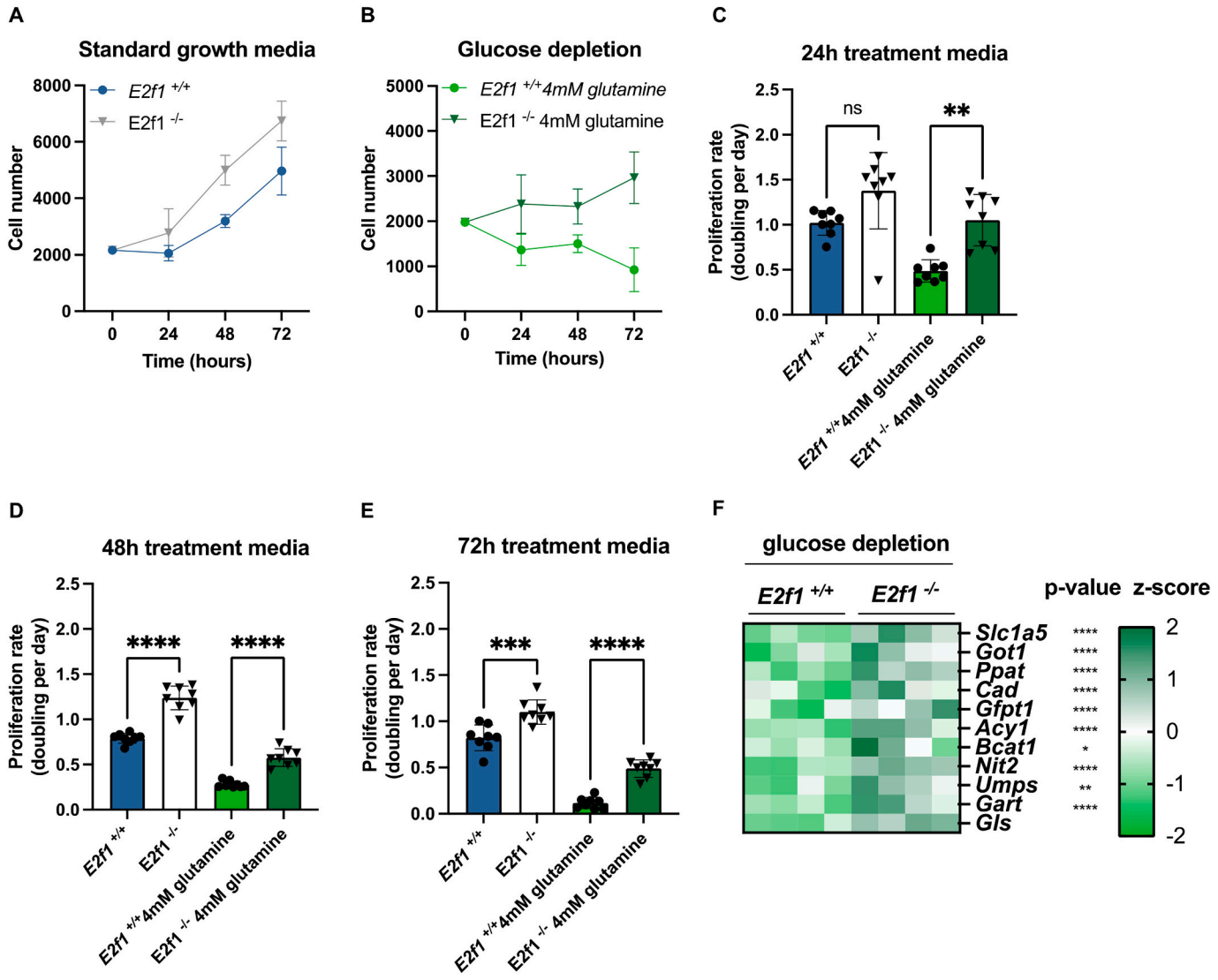

Fig. 3. Regulation of glutamine metabolism by E2F1 affects proliferation capacity.

transporter *Slc1a5* was validated by ChIP-qPCR analysis, which showed an increased binding of MYC upon E2F1 loss compared to MYC binding in control MEFs (Fig. 4C). Finally, knockdown of *Myc* in $E2f1^{+/+}$ and $E2f1^{-/-}$ MEFs (Fig. 4D-E) led to a significant reduction of *Slc1a5* expression in $E2f1^{-/-}$ MEFs (Fig. 4F).

(A) Validation of E2F1 binding at selected glutamine metabolic gene promoters such as solute carrier family member 5 (*SLC1A5)*, glutamic-pyruvic transaminase 1 (*GOT1)*, glutamic-pyruvic transaminase 2 (*GPT2*), phosphoribosyl pyrophosphate aminotransferase (*PPAT)* and carbamoyl-phosphate synthetase 2 (*CAD)* using ChIP-Seq tracks in HeLa and MCF7 cells. (B) E2F1 co-regulatory networks on promoter of cell cycle genes (KEGG id:hsa04110) and promoters of glutamine metabolic genes (KEGG id:hsa00250) using ChIP-seq data (ENCODE project, 61 unique transcription factors) in HeLa cells. (C) ChIP-qPCR on *Slc1a5* promoter in SV40-immortalized MEFs. Data are shown as mean ± SD, $n = 3$ independent experiments. (D-F) *Myc* knockdown in SV40-immortalized $E2f1^{+/+}$ and $E2f1^{-/-}$ MEFs. Data are shown as mean ± SD, $n = 10$ technical replicates from 3 independent experiments. Statistical significance was determined using ordinary one-way ANOVA with Turkey multiple comparisons and defined as $p < 0.01$ (**) and $p < 0.0001$ (****).

3.5. *The expression of glutamine metabolic genes is negatively-correlated with E2F1 and is associated with poor prognosis in human soft tissue sarcoma*

To validate the association between E2F1 and glutamine metabolism and its relevance in human tumors, we performed a correlation analysis using RNA-seq data from TCGA patients across 29 different cancer types. The signature of glutamine metabolic genes (KEGG id: hsa00250; restricted to direct target genes of E2F1 and MYC, which were differentially expressed in RNA-seq experiment) was examined and its enrichment score showed a negative correlation in certain cancer types including a significantly negative correlation in soft tissue sarcoma (STS) when compared with expression of *E2F1* (Fig. 5A). In STS, the glutamine signature score was also positively correlated with MYC expression, in agreement with its hypothesized role in regulating glutamine gene expression. In addition, a survival analysis comparing patients with high vs. low glutamine scores confirmed [50] that high expression of glutamine metabolic genes was indicative of poorer survival outcomes in STS (Fig. 5B). As previously described, one third of all spontaneously formed tumors in E2F1 knockout mice were found in the reproductive tract, including uterine sarcoma. Therefore, the uterine sarcoma cell lines SK-UT-1 was selected to silence E2F1 expression and a significant increase in the expression of glutamine metabolic genes such

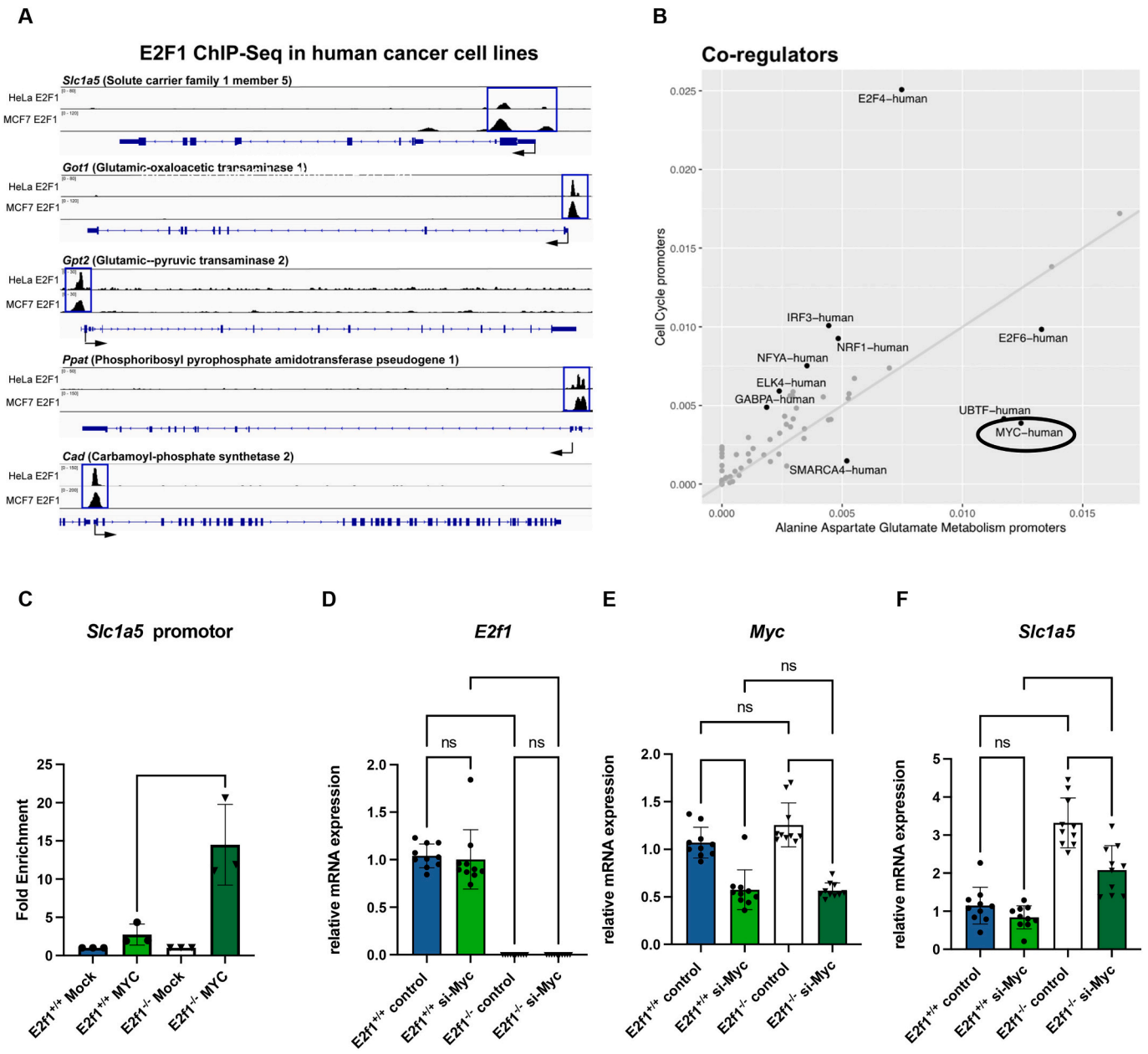

Fig. 4. Co-occupancy of E2F1 and MYC on the promoter of glutamine metabolic genes.

as *SLC1A5, GLS, GOT1* and *PPAT1* was observed by qPCR (Fig. 5C-D).

To further explore the role of E2F1 in SK-UT-1 cells, a E2F1-deficient cell line was generated by CRISPR/Cas9 technology (E2F1-ko and, as control, LacZ SK-UT-1 cells, Fig. 5E). We confirm that E2F1 knockout leads to elevated expression of glutamine transporter SLC1A5 and GLS levels (Fig. 5F). In addition, an increased cellular proliferation (Fig. 5G). and increased MYC binding to the promoter of *SLC1A5*, *CAD,* and *GOT1* by CUT&RUN-qPCR were observed upon loss of E2F1 (Fig. 5H).

Together, these analyses confirm our findings in a human cancer model and indicate that E2F1 loss drives an increase in glutamine metabolism in uterine sarcoma cells.

(A) Correlation analyses illustrating the Spearman correlation coefficients and *p*-values between the expression of E2F1/MYC (in log2 (TPM + 1) unit) across patients of each tumor type and the single-sample scores of the selected glutamine signature (genes of KEGG id: hsa00250, with E2F1 and MYC binding peak and which were differentially expressed in RNA-seq, see Supplementary table 1 computed using the R package 'singscore'. These scores quantify how much the genes in the signature are enriched among the most highly expressed genes. (B) KM plot showing the differences in overall survival between patients in low (bottom 25th percentiles of the signature score value) and high (top 25th percentiles) glutamine signature group for soft tissue sarcoma. Significance indicated by log-rank tests. (C) Analysis of *E2F1* mRNA expression (D) and mRNA expression of glutamine metabolic genes in human uterine sarcoma SK-UT-1 cell line $n = 8$ replicates performed in 3 independent experiments. (E) Western blot illustrating CRISPR/Cas9 generated E2F1 knockout (ko) in SK-UT-1 cell line. $n = 3$ replicates generated on independent days. (F) Analysis of *SLC1A5 and GLS* mRNA expression in LacZ and E2F1-ko SK-UT-1 cells. $n = 3$ replicates generated on independent days. (G) Cell growth of LacZ control (ctrl) and E2F1-ko SK-UT-1 cells was assessed in WST-1 assay. $n = 8$ technical replicates. Graph illustrates one representative experiment out of three independent experiments. (H) CUT&RUN qPCR analysis of MYC enrichment at *SLC1A5*, *CAD* and *GOT1* promoter in LacZ ctrl and E2F1-ko SK-UT-1 cells. CUT&RUN data show means of $2^{(\text{Delta Ct})}$ method, normalized to *HPRT1* and *VCAM1* control loci, as well as to the corresponding IgG

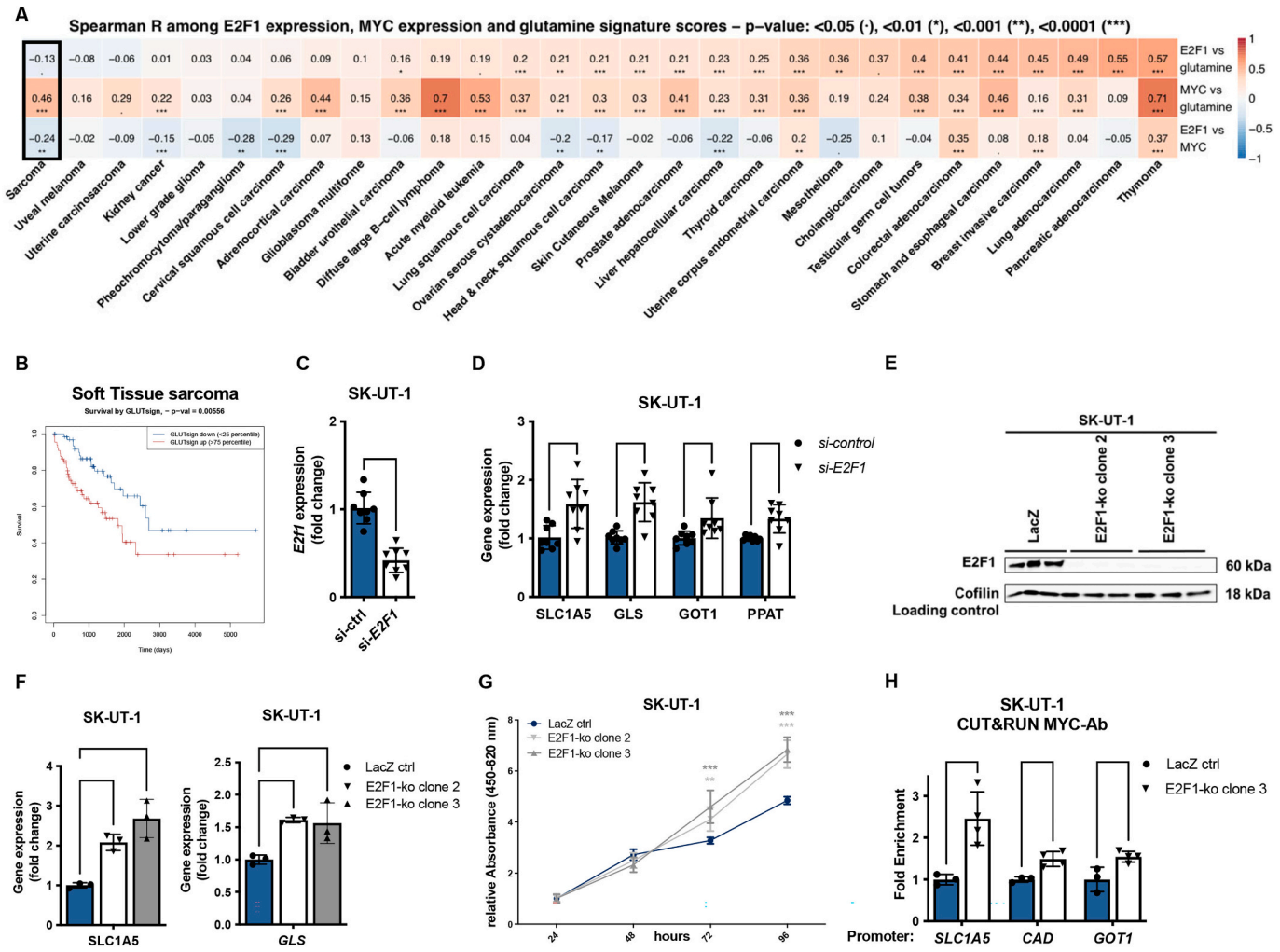

Fig. 5. The expression of glutamine metabolic genes is negatively-correlated with E2F1 and is associated with poor prognosis in human soft tissue sarcoma.

control. $n = 3$–4 replicates representative of 2 independent experiments. All data shows mean ± SD. Statistical significance was determined by unpaired Student's two-tailed *t*-test or an ordinary one-way ANOVA with Dunnett's multiple comparisons test defined as $p < 0.05$ (*), $p < 0.01$ (**), $p < 0.001$ (***), and $p < 0.0001$ (****).

4. Discussion

Previous studies have demonstrated a dual role of E2F1 transcription factor as an oncogene and tumor suppressor. While an increase in E2F activity is commonly found in many human cancers [10], E2F1's tumor suppressive properties have become evident by the observation that E2f1-deficient mice develop spontaneous tumors between 8 and 18 months of age. The fact that mice lacking E2f1 show an increase in tumor incidence suggests that E2F1 can also function as a tumor suppressor [13].

Mechanistically, a failure of the protective apoptotic pathway was suggested, eventually resulting in elevated proliferation and increased tumorigenesis as cells that might otherwise go on to form a tumor are not eliminated and therefore accumulate additional oncogenic alterations. However, the observation that inactivation of E2f1 accelerates tumorigenesis in mice expressing MYC under the control of an epithelial-specific keratin 5 promoter (K5 *Myc* mice) while at the same time increasing apoptosis in transgenic epidermis and tumors does not support the model in which E2F1 suppresses tumor development by inducing apoptosis [51]. This suggests that E2F1 might have additional tumor suppressive activities.

The ability of E2F1 to affect the expression of diverse collections of genes including metabolic processes, rather than just cellular proliferation and apoptosis, may also contribute to its roles as a tumor suppressor. However, the mechanisms of how E2F1 affects metabolism in these tumors and how it contributes to tumor formation has not been determined yet and warrants a detailed investigation of the molecular mechanism how signaling through CDK4/6-RB-E2F pathway controls glutamine metabolism.

Our data identified metabolic control and reprogramming of glutamine metabolism that follows E2F1 depletion. The glutamine transporter, SLC1A5, was one of the most up-regulated genes upon E2F1 knockout in MEFs. In addition, *E2f1*$^{-/-}$ MEFs are more efficient in metabolizing glutamine, thereby producing important intermediates for cellular proliferation.

Furthermore, ChIP-seq analysis showed a direct binding of E2F1 to the promoters of glutamine metabolic genes, implying a direct or indirect E2F1-mediated transcriptional repression of the cancer hallmark glutamine metabolism. Several levels of regulation of E2F1 activity have been described. The dual nature of E2F sites to positively or negatively regulate transcription may allow E2F1 to perform vastly different tasks depending on the promoter context in which E2F sites are located. E2F1 can function as a transcriptional repressor either through interaction with negative regulators including pRB [52–55], p53 [56], as well as alone [57–59] or through association with specific co-factors, such as HDAC1 [60], DNMT1 [59], KDMA4 [61] and BIN1 [62]. The loss of

E2F1 and the subsequent loss of the E2F1 repressor complexes may allow other transcription factors to bind to those binding sites on the promoter. Therefore, we studied which transcription factor showed a co-occupancy with E2F1 on the promoter of glutamine metabolic genes and compared them to the promoter of classical cell cycle targets. The transcription factor that showed the highest co-occupancy on glutamine metabolic gene promoter and not on cell cycle promoters was the oncogene MYC.

The transcription factor MYC in conjunction with the heterodimer partner protein MAX binds to *E*-box sequence elements and regulates several biological activities that contribute to tumorigenesis including glutaminolytic metabolism [63]. The functional relationship between MYC and E2F1 is context dependent and appears to be complex. A cooperation of E2F1 inactivation and MYC overexpression has been identified as a specific oncogenic alteration to promote tumorigenesis in K5 *Myc* mice crossed with E2f1-null mice [51]. Additionally, it has been reported that modulating upstream pathways of E2F1 such as inhibition of CDK4/6 in HCT116 cells prevents the phosphorylation of MYC at Thr58 and Ser62 and ensuing its ubiquitin-proteasome-dependent turnover. This leads to accumulation of MYC protein and subsequent upregulation of the gene networks orchestrated by MYC [19]. Together with our data, there is increasing evidence for a complex link between MYC and the CDK4/6-Rb-E2F pathway that needs further investigation in certain human types of cancer.

Our observations in MEFs have been cross validated with analyses of transcriptomic profiles in 29 different human cancer types and highlighted STSs as a specific cancer type that showed a negative correlation between E2F1 and certain glutamine metabolic genes.

STSs are a rare group of heterogeneous mesenchymal cancers originating from connective tissue, now classified into >100 distinct subtypes based on their tissue of origin, genetic alterations, and age of occurrence. STSs account for 1 % of all adult cancers and due to their rarity and heterogeneity, these diseases remain relatively understudied - making new therapeutic targets necessary and challenging [64,65].

In accordance with the literature, we demonstrated that high expression of glutamine metabolic genes is closely associated with poor prognoses of patients [50,66]. Moreover, tumor development was found to be accelerated in the absence of E2F1 in reproductive tract sarcomas, including uterine sarcoma, which represent one-third of all the tumors isolated from E2F1$^{-/-}$ animals. Although, a broad spectrum of tumors developed in mice lacking E2F1 including lung tumors, lymphomas, und other tumor types found at lower frequency [13], our restricted analysis focusing on glutamine gene expression negatively correlated with E2F1 expression identified a specific importance in STS. Thus, we selected a cell line of leiomyosarcoma, which represents the most common type of uterine sarcoma [67], to validate our results in a human cancer model and confirm a significant increase in the expression of glutamine metabolic genes, increased proliferation and increased MYC binding to promoters of SLC1A5, GOT1 and CAD upon E2F1 knockout.

In conclusion, these data reveal a novel function of E2F1 in rewiring cellular metabolism through a cooperation with MYC to regulate glutamine metabolism-related genes at the transcriptional level. These findings seem to be relevant specifically for uterine sarcoma, encouraging testing novel pre-clinical strategies to tackle these metabolic pathways with pharmacological interventions.

Funding source.

K.H. was supported by the Austrian Science Fund (FWF) grant J4597-B. We acknowledge the Swiss National Science Foundation grant (31003A_143369) to L.F. L.F. group and S.G. salary and project were supported by Swiss National Science Foundation grant (310030_207688) and Science Novartis Foundation grant (#22B129). M.P.'s research was supported by the Austrian Science Fund (W1226, P35975-B).

Research data

GEO record: GSE230129.

CRediT authorship contribution statement

Katharina Huber: Conceptualization, Writing- original draft, Writing -review & editing, Investigation, Methodology, Data curation, Formal analysis. **Albert Giralt:** Formal analysis, Investigation, Methodology. **René Dreos:** Data curation. **Helene Michenthaler:** Investigation, Methodology. **Sarah Geller:** Investigation, Methodology. **Valentin Barquissau:** Formal analysis, Investigation. **Dorian V. Ziegler:** Formal analysis, Investigation, Methodology. **Daniele Tavernari:** Data curation, Formal analysis. **Hector Gallart-Ayala:** Formal analysis, Methodology. **Katarina Krajina:** Formal analysis, Investigation. **Katharina Jonas:** Data curation, Investigation, Writing – review & editing. **Giovanni Ciriello:** Data curation. **Julijana Ivanisevic:** Data curation, Formal analysis, Methodology. **Andreas Prokesch:** Formal analysis, Investigation. **Martin Pichler:** Conceptualization, Resources. **Lluis Fajas:** Conceptualization, Investigation, Project administration, Supervision, Validation, Writing – original draft, Writing – review & editing.

Declaration of Generative AI and AI-assisted technologies in the writing process

During the preparation of this work the author(s) did not used AI-assisted tool or services.

Declaration of competing interest

The authors declare no competing interests, except A.G., who is an employee of Société des Produits Nestlé S.A.

Data availability

Data will be made available on request.

Acknowledgements

We thank our colleagues from the GTF (Julien Marquis, Johann Weber, Hannes Richter and Viviane Praz) who performed the library preparation, sequencing, the quality controls and data processing for the RNA-seq experiment. We acknowledge all of the members of the Fajas and Pichler laboratory for support and discussions. SV40LargeTantigen. lti-neo was a kind gift from the Widmann lab [24]. We acknowledge that *E2f1*$^{+/+}$ and *E2f1*$^{-/-}$ MEFs have been isolated for a previous project of the Fajas laboratory by I. C. Lopez-Meija [23]. We acknowledge that the sarcoma cell line has been provided by Beate Rinner and technical support of Djenana Vejzovic and Sophie Kienreich. Illustrations have been created in Biorender.com.

Appendix A. Supplementary data

Supplementary data to this article can be found online at https://doi.org/10.1016/j.bbamcr.2024.119721.

References

[1] D. Hanahan, R.A. Weinberg, Hallmarks of cancer: the next generation, Cell 144 (2011) 646–674, https://doi.org/10.1016/j.cell.2011.02.013.
[2] D. Hanahan, Hallmarks of Cancer: new dimensions, Cancer Discov. 12 (2022) 31–46, https://doi.org/10.1158/2159-8290.Cd-21-1059.
[3] R.J. DeBerardinis, N.S. Chandel, Fundamentals of cancer metabolism, Sci Adv 2 (2016) e1600200, https://doi.org/10.1126/sciadv.1600200.
[4] D.R. Wise, C.B. Thompson, Glutamine addiction: a new therapeutic target in cancer, Trends Biochem. Sci. 35 (2010) 427–433, https://doi.org/10.1016/j.tibs.2010.05.003.

[5] N.P. Curthoys, M. Watford, Regulation of glutaminase activity and glutamine metabolism, Annu. Rev. Nutr. 15 (1995) 133–159, https://doi.org/10.1146/annurev.nu.15.070195.001025.
[6] R.W. Moreadith, A.L. Lehninger, The pathways of glutamate and glutamine oxidation by tumor cell mitochondria. Role of mitochondrial NAD(P)+−dependent malic enzyme, J. Biol. Chem. 259 (1984) 6215–6221.
[7] J. Son, et al., Glutamine supports pancreatic cancer growth through a KRAS-regulated metabolic pathway, Nature 496 (2013) 101–105, https://doi.org/10.1038/nature12040.
[8] J. Zhang, N.N. Pavlova, C.B. Thompson, Cancer cell metabolism: the essential role of the nonessential amino acid, glutamine, EMBO J. 36 (2017) 1302–1315, https://doi.org/10.15252/embj.201696151.
[9] M.G. Vander Heiden, Targeting cancer metabolism: a therapeutic window opens, Nat. Rev. Drug Discov. 10 (2011) 671–684, https://doi.org/10.1038/nrd3504.
[10] H.Z. Chen, S.Y. Tsai, G. Leone, Emerging roles of E2Fs in cancer: an exit from cell cycle control, Nat. Rev. Cancer 9 (2009) 785–797, https://doi.org/10.1038/nrc2696.
[11] S. Lim, P. Kaldis, Cdks, cyclins and CKIs: roles beyond cell cycle regulation, Development 140 (2013) 3079–3093, https://doi.org/10.1242/dev.091744.
[12] K. Huber, A. Mestres-Arenas, L. Fajas, L.C. Leal-Esteban, The multifaceted role of cell cycle regulators in the coordination of growth and metabolism, FEBS J. 288 (2021) 3813–3833, https://doi.org/10.1111/febs.15586.
[13] L. Yamasaki, et al., Tumor induction and tissue atrophy in mice lacking E2F-1, Cell 85 (1996) 537–548, https://doi.org/10.1016/s0092-8674(00)81254-4.
[14] S.J. Field, et al., E2F-1 functions in mice to promote apoptosis and suppress proliferation, Cell 85 (1996) 549–561, https://doi.org/10.1016/s0092-8674(00)81255-6.
[15] A.C. Mandigo, et al., RB/E2F1 as a master regulator of Cancer cell metabolism in advanced disease, Cancer Discov. 11 (2021) 2334–2353, https://doi.org/10.1158/2159-8290.Cd-20-1114.
[16] M.R. Reynolds, et al., Control of glutamine metabolism by the tumor suppressor Rb, Oncogene 33 (2014) 556–566, https://doi.org/10.1038/onc.2012.635.
[17] S. Qie, et al., Targeting glutamine-addiction and overcoming CDK4/6 inhibitor resistance in human esophageal squamous cell carcinoma, Nat. Commun. 10 (2019) 1296, https://doi.org/10.1038/s41467-019-09179-w.
[18] J. Franco, U. Balaji, E. Freinkman, A.K. Witkiewicz, E.S. Knudsen, Metabolic reprogramming of pancreatic Cancer mediated by CDK4/6 inhibition elicits unique vulnerabilities, Cell Rep. 32 (2020) 107793, https://doi.org/10.1016/j.celrep.2020.107793.
[19] M. Tarrado-Castellarnau, et al., De novo MYC addiction as an adaptive response of cancer cells to CDK4/6 inhibition, Mol. Syst. Biol. 13 (2017) 940, https://doi.org/10.15252/msb.20167321.
[20] L.R. Conroy, et al., Palbociclib treatment alters nucleotide biosynthesis and glutamine dependency in A549 cells, Cancer Cell Int. 20 (2020) 280, https://doi.org/10.1186/s12935-020-01357-x.
[21] B.N. Nicolay, et al., Loss of RBF1 changes glutamine catabolism, Genes Dev. 27 (2013) 182–196, https://doi.org/10.1101/gad.206227.112.
[22] P.D. Denechaud, et al., E2F1 mediates sustained lipogenesis and contributes to hepatic steatosis, J. Clin. Invest. 126 (2016) 137–150, https://doi.org/10.1172/jci81542.
[23] I.C. Lopez-Mejia, et al., CDK4 phosphorylates AMPKα2 to inhibit its activity and repress fatty acid oxidation, Mol. Cell 68 (2017), https://doi.org/10.1016/j.molcel.2017.09.034, 336-349.e336.
[24] A. Annibaldi, A. Dousse, S. Martin, J. Tazi, C. Widmann, Revisiting G3BP1 as a RasGAP binding protein: sensitization of tumor cells to chemotherapy by the RasGAP 317-326 sequence does not involve G3BP1, PloS One 6 (2011) e29024, https://doi.org/10.1371/journal.pone.0029024.
[25] K.J. Livak, T.D. Schmittgen, Analysis of relative gene expression data using real-time quantitative PCR and the 2(-Delta Delta C(T)) method, Methods 25 (2001) 402–408, https://doi.org/10.1006/meth.2001.1262.
[26] K. Jonas, et al., MiR-4649-5p acts as a tumor-suppressive microRNA in triple negative breast cancer by direct interaction with PIP5K1C, thereby potentiating growth-inhibitory effects of the AKT inhibitor capivasertib, Breast Cancer Res. 25 (2023) 119, https://doi.org/10.1186/s13058-023-01716-2.
[27] A. Dobin, et al., STAR: ultrafast universal RNA-seq aligner, Bioinformatics 29 (2013) 15–21, https://doi.org/10.1093/bioinformatics/bts635.
[28] S. Anders, P.T. Pyl, W. Huber, HTSeq–a Python framework to work with high-throughput sequencing data, Bioinformatics 31 (2015) 166–169, https://doi.org/10.1093/bioinformatics/btu638.
[29] M.I. Love, W. Huber, S. Anders, Moderated estimation of fold change and dispersion for RNA-seq data with DESeq2, Genome Biol. 15 (2014) 550, https://doi.org/10.1186/s13059-014-0550-8.
[30] A. Liberzon, et al., The molecular signatures database (MSigDB) hallmark gene set collection, Cell Syst. 1 (2015) 417–425, https://doi.org/10.1016/j.cels.2015.12.004.
[31] G. Korotkevich, et al., Fast gene set enrichment analysis, bioRxiv (2021) 060012, https://doi.org/10.1101/060012.
[32] G. Yu, Q.Y. He, ReactomePA: an R/Bioconductor package for reactome pathway analysis and visualization, Mol. Biosyst. 12 (2016) 477–479, https://doi.org/10.1039/c5mb00663e.
[33] J. Ivanisevic, et al., Toward 'omic scale metabolite profiling: a dual separation-mass spectrometry approach for coverage of lipid and central carbon metabolism, Anal. Chem. 85 (2013) 6876–6884, https://doi.org/10.1021/ac401140h.
[34] H. Gallart-Ayala, et al., A global HILIC-MS approach to measure polar human cerebrospinal fluid metabolome: exploring gender-associated variation in a cohort of elderly cognitively healthy subjects, Anal. Chim. Acta 1037 (2018) 327–337, https://doi.org/10.1016/j.aca.2018.04.002.
[35] F.S. Midani, M.L. Wynn, S. Schnell, The importance of accurately correcting for the natural abundance of stable isotopes, Anal. Biochem. 520 (2017) 27–43, https://doi.org/10.1016/j.ab.2016.12.011.
[36] C. Guijas, et al., METLIN: a technology platform for identifying knowns and unknowns, Anal. Chem. 90 (2018) 3156–3164, https://doi.org/10.1021/acs.analchem.7b04424.
[37] M. Jain, et al., Metabolite profiling identifies a key role for glycine in rapid cancer cell proliferation, Science 336 (2012) 1040–1044, https://doi.org/10.1126/science.1218595.
[38] I. Roci, et al., Metabolite profiling and stable isotope tracing in sorted subpopulations of mammalian cells, Anal. Chem. 88 (2016) 2707–2713, https://doi.org/10.1021/acs.analchem.5b04071.
[39] A.J. Kueh, M.J. Herold, Using CRISPR/Cas9 Technology for Manipulating Cell Death Regulators, Methods Mol. Biol. 1419 (2016) 253–264, https://doi.org/10.1007/978-1-4939-3581-9_18.
[40] A. Panday, R. Elango, N.A. Willis, R. Scully, A modified CUT&RUN-seq technique for qPCR analysis of chromatin-protein interactions, STAR Protoc 3 (2022) 101529, https://doi.org/10.1016/j.xpro.2022.101529.
[41] P.J. Skene, J.G. Henikoff, S. Henikoff, Targeted in situ genome-wide profiling with high efficiency for low cell numbers, Nat. Protoc. 13 (2018) 1006–1019, https://doi.org/10.1038/nprot.2018.015.
[42] R. Dreos, G. Ambrosini, R. Groux, R. Cavin Périer, P. Bucher, The eukaryotic promoter database in its 30th year: focus on non-vertebrate organisms, Nucleic Acids Res. 45 (2017) D51–D55, https://doi.org/10.1093/nar/gkw1069.
[43] E. Cerami, et al., The cBio cancer genomics portal: an open platform for exploring multidimensional cancer genomics data, Cancer Discov. 2 (2012) 401–404, https://doi.org/10.1158/2159-8290.Cd-12-0095.
[44] M. Kanehisa, S. Goto, KEGG: Kyoto encyclopedia of genes and genomes, Nucleic Acids Res. 28 (2000) 27–30, https://doi.org/10.1093/nar/28.1.27.
[45] M. Foroutan, et al., Single sample scoring of molecular phenotypes, BMC Bioinformatics 19 (2018) 404, https://doi.org/10.1186/s12859-018-2435-4.
[46] T.M. Therneau, A Package for Survival Analysis in R, 2020.
[47] E. Blanchet, et al., E2F transcription factor-1 regulates oxidative metabolism, Nat. Cell Biol. 13 (2011) 1146–1152, https://doi.org/10.1038/ncb2309.
[48] Q. Xie, et al., E2F transcription factor 1 regulates cellular and organismal senescence by inhibiting Forkhead box O transcription factors, J. Biol. Chem. 289 (2014) 34205–34213, https://doi.org/10.1074/jbc.M114.587170.
[49] R.J. DeBerardinis, et al., Beyond aerobic glycolysis: transformed cells can engage in glutamine metabolism that exceeds the requirement for protein and nucleotide synthesis, Proc. Natl. Acad. Sci. U. S. A. 104 (2007) 19345–19350, https://doi.org/10.1073/pnas.0709747104.
[50] P. Lee, et al., Targeting glutamine metabolism slows soft tissue sarcoma growth, Nat. Commun. 11 (2020) 498, https://doi.org/10.1038/s41467-020-14374-1.
[51] R.J. Rounbehler, P.M. Rogers, C.J. Conti, D.G. Johnson, Inactivation of E2f1 enhances tumorigenesis in a Myc transgenic model, Cancer Res. 62 (2002) 3276–3281.
[52] A. Brehm, et al., Retinoblastoma protein recruits histone deacetylase to repress transcription, Nature 391 (1998) 597–601, https://doi.org/10.1038/35404.
[53] E.K. Flemington, S.H. Speck, W.G. Kaelin Jr., E2F-1-mediated transactivation is inhibited by complex formation with the retinoblastoma susceptibility gene product, Proc. Natl. Acad. Sci. U. S. A. 90 (1993) 6914–6918, https://doi.org/10.1073/pnas.90.15.6914.
[54] C. Hagemeier, A. Cook, T. Kouzarides, The retinoblastoma protein binds E2F residues required for activation in vivo and TBP binding in vitro, Nucleic Acids Res. 21 (1993) 4998–5004, https://doi.org/10.1093/nar/21.22.4998.
[55] L. Magnaghi-Jaulin, et al., Retinoblastoma protein represses transcription by recruiting a histone deacetylase, Nature 391 (1998) 601–605, https://doi.org/10.1038/35410.
[56] D.J. O'Connor, et al., Physical and functional interactions between p53 and cell cycle co-operating transcription factors, E2F1 and DP1, EMBO J. 14 (1995) 6184–6192, https://doi.org/10.1002/j.1460-2075.1995.tb00309.x.
[57] D.L. Crowe, D.C. Nguyen, K.J. Tsang, S. Kyo, E2F-1 represses transcription of the human telomerase reverse transcriptase gene, Nucleic Acids Res. 29 (2001) 2789–2794, https://doi.org/10.1093/nar/29.13.2789.
[58] R. Croxton, Y. Ma, L. Song, E.B. Haura, W.D. Cress, Direct repression of the Mcl-1 promoter by E2F1, Oncogene 21 (2002) 1359–1369, https://doi.org/10.1038/sj.onc.1205157.
[59] J.N. Davis, et al., Elevated E2F1 inhibits transcription of the androgen receptor in metastatic hormone-resistant prostate cancer, Cancer Res. 66 (2006) 11897–11906, https://doi.org/10.1158/0008-5472.Can-06-2497.
[60] Z. Lu, et al., E2F-HDAC complexes negatively regulate the tumor suppressor gene ARHI in breast cancer, Oncogene 25 (2006) 230–239, https://doi.org/10.1038/sj.onc.1209025.
[61] L.Y. Wang, et al., KDM4A Coactivates E2F1 to regulate the PDK-dependent metabolic switch between mitochondrial oxidation and glycolysis, Cell Rep. 16 (2016) 3016–3027, https://doi.org/10.1016/j.celrep.2016.08.018.
[62] W.P. Folk, et al., Loss of the tumor suppressor BIN1 enables ATM Ser/Thr kinase activation by the nuclear protein E2F1 and renders cancer cells resistant to cisplatin, J. Biol. Chem. 294 (2019) 5700–5719, https://doi.org/10.1074/jbc.RA118.005699.
[63] C. Lourenco, et al., MYC protein interactors in gene transcription and cancer, Nat. Rev. Cancer 21 (2021) 579–591, https://doi.org/10.1038/s41568-021-00367-9.

[64] A. Dufresne, M. Brahmi, M. Karanian, J.Y. Blay, Using biology to guide the treatment of sarcomas and aggressive connective-tissue tumours, Nat. Rev. Clin. Oncol. 15 (2018) 443–458, https://doi.org/10.1038/s41571-018-0012-4.
[65] B.S. Taylor, et al., Advances in sarcoma genomics and new therapeutic targets, Nat. Rev. Cancer 11 (2011) 541–557, https://doi.org/10.1038/nrc3087.
[66] J. Zou, et al., Glutamine metabolism regulators associated with Cancer development and the tumor microenvironment: a Pan-Cancer multi-omics analysis, Genes (Basel) 12 (2021), https://doi.org/10.3390/genes12091305.
[67] S. George, C. Serrano, M.L. Hensley, I. Ray-Coquard, Soft tissue and uterine Leiomyosarcoma, J. Clin. Oncol. 36 (2018) 144–150, https://doi.org/10.1200/jco.2017.75.9845.